Ion Trapping with Fast-Response Ion-Selective Microelectrodes Enhances Detection of Extracellular Ion Channel Gradients

Mark A. Messerli,* Leon P. Collis, and Peter J. S. Smith
BioCurrents Research Center, Cell Dynamics Program, Marine Biological Laboratory, Woods Hole, Massachusetts 02543

ABSTRACT   Previously, functional mapping of channels has been achieved by measuring the passage of net charge and of specific ions with electrophysiological and intracellular fluorescence imaging techniques. However, functional mapping of ion channels using extracellular ion-selective microelectrodes has distinct advantages over the former methods. We have developed this method through measurement of extracellular K^+ gradients caused by efflux through Ca^{2+}-activated K^+ channels expressed in Chinese hamster ovary cells. We report that electrodes constructed with short columns of a mechanically stable K^+-selective liquid membrane respond quickly and measure changes in local $[K^+]$ consistent with a diffusion model. When used in close proximity to the plasma membrane (<4 μm), the ISMs pose a barrier to simple diffusion, creating an ion trap. The ion trap amplifies the local change in $[K^+]$ without dramatically changing the rise or fall time of the $[K^+]$ profile. Measurement of extracellular K^+ gradients from activated rSlo channels shows that rapid events, 10–55 ms, can be characterized. This method provides a noninvasive means for functional mapping of channel location and density as well as for characterizing the properties of ion channels in the plasma membrane.

INTRODUCTION

Plasma membrane ion channels are involved with maintaining ionic balance and controlling ionic changes for signaling pathways. Short-term blockade or inactivation of channels destroys signaling pathways, whereas relatively long-term inactivation interferes with ionic homeostasis and cell viability (1). With the aid of voltage-clamp methods, parameters such as conductance, permeability, and mode of activation have been characterized for many different types of channels. However, current methods for the functional mapping of the location of ion channels on cells are tedious. There are at least three different types of methods that have been used to map the functional distribution of ion channels: 1), voltage clamp of channels using loose patch clamp (reviewed by Roberts and Almers (2)); 2), scanning ion conductance (SICM) using whole-cell voltage clamp with a scanning current-passing electrode (3); and 3), monitoring of intracellular fluorescent ion indicators (4,5). The first two methods take advantage of the measurement of current caused by the rapid movement of charged ions across the plasma membrane, although the measured current will be from any number of channels with different ionic permeabilities. Additional experimental manipulations are needed to obtain channel identity, including ion substitution and/or removal, addition of specific pharmacological blockers, and identification of activation or reversal potentials. Loose patch-clamp methods are difficult to use on flattened morphologically distinct regions of cells compared to rounded-up regions and generally are not practical on small cells (2). Ion substitution was used in conjunction with SICM to functionally localize K_{ATP} channels on

cardiac myocytes. Specifically, K^+ and other K_{ATP} permeant ions were removed completely from both intracellular and extracellular solutions. K^+ was supplied to the channel via a scanning extracellular pipette filled with 1M K^+ (3). The success of this method was dependent on nonphysiological ionic conditions and whole-cell voltage clamp. The third method, the use of fluorescent ion indicators to monitor ion concentration changes after passage through channels, allows long-term study of ion channels. However, it is at best restricted to Ca^{2+} and H^+ influx through ion channels because of the low intracellular concentration of the ions as well as the high selectivity and sensitivity of their fluorescent indicators compared to other inorganic ion indicators (6).

Based on the insight given by these methods, it became apparent that extracellular ion-selective microelectrodes (ISMs) could be used for functional mapping of ion channels and also for characterization of the channels. Extracellular ISMs have been used to measure steady and dynamic changes in extracellular ion gradients near single cells and tissues that arise as a result of ion passage across the plasma membrane via channels, transporters, or exchangers (7,8). Similar to fluorescent indicators, ISMs possess an inherent selectivity enabling measurement of channel activity for channels passing a specific ion in the presence of active channels passing other ions. However, they possess a greater signal/noise ratio than their corresponding fluorescent ion indicators, are useful over a wider dynamic range, and exist for a wide range of inorganic ions. Extracellular ISMs can be used in a scanning mode similar to the SICM and loose patch discussed above but do not contact the cell-like loose patch and can be used under more physiologically relevant conditions than those used with SICM.

In this report, we used fast-response K^+-selective microelectrodes to capture rapid (10–55 ms duration) extracellular

K$^+$ transients that arise from the activity of Ca^{2+}-activated K$^+$ ion channels. We also report that ion trapping by the ISM increases the magnitude of the single-channel gradients, making it easier to detect and map the gradients.

MATERIALS AND METHODS

Electrode construction

Fast-response ISMs were fabricated by simple modifications to the previous design (9). The fast-design K$^+$-selective electrode incorporated a more mechanically stable liquid membrane that enabled construction with stable shorter columns, ≤ 10 μm. The K$^+$-selective liquid membrane was made similar to the K$^+$-selective mixture 60398 (Sigma-Aldrich (Fluka), St. Louis, MO), with the exception that 1,2-dimethyl-3-nitrobenzene was replaced with 2-nitrophenyl octyl ether. The valinomycin-based liquid membranes have >3 orders of magnitude selectivity for K$^+$ over other common cations including Na$^+$, H$^+$, Ca^{2+}, and Mg^{2+} (10). Microelectrode bodies for the liquid membrane were pulled from both borosilicate (WPI, Sarasota, FL) and aluminosilicate glass (Sutter Instruments, Novato, CA). Borosilicate (1.5/0.84 and 2.0/1.12 mm OD/ID) and aluminosilicate (1.5/1.0 mm OD/ID) glass capillaries were pulled to obtain tips of 2–3 μm inner diameter. This resulted in tip wall thickness of 200 and 300 nm for the 1.5 and 2.0 mm OD pipettes, respectively. Stable ISMs with short columns of ionophore were not always possible with borosilicate glass but were made more consistently with aluminosilicate glass. Pulled pipettes were silanized with the vapor method by first drying glass at 230–240°C for 20 min under vacuum 28 in. Hg. The evacuated oven was purged with argon, and the electrodes were introduced to 20 μL of *N,N*-dimethyltrimethylsilylamine (Sigma-Aldrich (Fluka)) in an enclosed metal box at 230–240°C for 20 min. After silanization, pipettes were stored in a bell jar with desiccant in the bottom. Electrical connection was made with a Ag/AgCl wire connected to a backfilling solution of 100 mM KCl, 10 mM HEPES, pH 7.4.

Concentric ISMs were constructed according to previous designs (11,12). Borosilicate glass with a filament (1.0/0.75 mm OD/ID) was inserted and immobilized into a pulled and silanized outer borosilicate pipette (1.5/1.12 mm OD/ID). Immobilization was achieved with a UV-curing glue, Norland Optical Adhesive No. 74 (Norland Products, Cranbury, NJ). The tip of the inner pipette was within 10 μm of the tip of the outer pipette. The inner pipette was filled with backfilling solution before the liquid membrane was tip loaded into the outer pipette. The liquid membrane was equilibrated with 100 mM KCl before loading as previously described (13).

ISMs measure ionic activity. However, we instead refer to ISMs as measuring ionic concentration, as ionic activity is directly proportional to ion concentration via the activity coefficient, and the changes that occur to the activity coefficient as a result of changes in ionic strength are negligible during our measurements. We reserve the term active or activity to discuss the state of the ion channels.

Cell maintenance and handling

Chinese hamster ovary (CHO) cells stably expressing the Ca^{2+}-activated K$^+$ channel, rSlo, were maintained in Iscove's Modified Dulbecco's Medium with 10% FBS, HT supplement, and 1% of 10 K IU penicillin streptomycin (Invitrogen, Carlsbad, CA). During recordings, medium was replaced with a physiological saline containing (in mM) 140 NaCl, 5 CaCl$_2$, 29 glucose, 25 HEPES, pH 7.2, with 0.3 KCl. Electrodes used for whole-cell voltage clamp were filled with (in mM) 32.5 KCl, 97.5 K$^+$ gluconate, 5 EGTA, 10 HEPES, pH 7.2, with either 2.5 or 3.5 CaCl$_2$ resulting in a final free [Ca^{2+}] of ~200 and 400 nM, respectively, calculated with WEBMAXC Standard (14) (http://www.stanford.edu/~cpatton/maxc.html).

K$^+$ gradients were measured near the plasma membrane of CHO cells held under whole-cell voltage clamp with varying [Ca^{2+}]$_i$. Iberiotoxin (300 nM) was added while clamping [Ca^{2+}]$_i$ to 400 nM to capture single-channel gradients at a range of applied voltages. Voltage clamp was performed with an

Axoclamp 200B amplifier while K$^+$ gradients were measured using an Axoclamp 2B amplifier with the 0.0001 H headstage. Additional amplification was provided by a Warner Instruments LPF-100B (Hamden, CT). An offset was applied to the ISM signal to apply gain and maintain the signal within the dynamic range of the LPF-100B amplifier.

Ion gradient modeling and analysis

Construction of a realistic ISM

To assess the extent to which an ISM can affect the diffusion profile of K$^+$ ions, a three-dimensional (3D) approach to modeling the movements of ions was undertaken. First it was necessary to incorporate a 3D representation of a typical ISM into the model environment. It was only necessary to incorporate a 10 μm length of the ISM from the tip, as we were analyzing the diffusion of ions from a single ion channel over millisecond time periods. Typical dimensions of tip diameter and taper angle were extracted from scanning electron micrographs of ISMs and used to construct a 3D model using the open-source 3D generation suite, Blender (version 2.45). This software was run on a Linux platform (Fedora release 8) on a HP xw4400 workstation with 2 GB RAM and a 2.1 GHz processor. ISMs were translated and rotated within the 3D environment to assess the effect of orientation and separation distance on the diffusion profile of ions.

Simulation of an ion channel

We used a Monte-Carlo method for simulating the Brownian motion of ions from a point source in a 3D environment. For this purpose, the Model Description Language used within MCell (version 3.0 (15,16)) was used to simulate the diffusion and random walk of K$^+$ ions from a point source (a 270 pS K$^+$ channel) with a diffusion coefficient of 1.96×10^{-5} cm^2 s^{-1}. To decrease simulation time, the extracellular background concentration of K$^+$ was left at zero. Our graphs report the change to the local [K$^+$]. The code was written and executed using the same platform described above. Simulation time was optimized by partitioning the 3D environment into 0.2-μm cubes and by increasing the time step to 10 μs. Although this reduced the simulation time significantly, no significant change in diffusion profile resulted from optimizing these parameters (data not shown). The simulation generated ions at a rate of 6.75×10^7 s^{-1} from a single point source. To further reduce simulation time, a 10 μm boundary box enclosed the simulation, and any ion that contacted the box was deemed to have left the simulation space and was removed from the simulation. This had no effect on diffusion profiles sampled at ≤ 3 μm from the point source (data not shown). The boundary box was omitted for the diffusion profiles collected at 10 μm from the source. After a set channel open time (10–50 ms), the simulation was stopped, and simulation data were checkpointed to a second simulation program where the ion channel was closed.

Ion concentration was assessed using MCell sample boxes to count ions. Sample boxes were generated using Blender and consisted of either a 100-nm-thick disk covering the aperture of the ISM or a 100-nm-diameter sphere at the center of the ISM aperture. The disk sample box was a reflection of the actual ion concentration that the ISM would detect and thus convert to a corresponding change in the electrode's Nernstian voltage. However, ion concentration was dependent on the orientation of the cylinder. To eliminate the angle of the sample box as a variable, a sphere was used at varying distances from the point source to calculate ion concentration. The separation distance between the sample boxes and the point source was adjusted at incrementing distances from 0.2 μm to 10 μm. To reduce simulation noise and obtain an average of simulation trials, the software was executed with different initial seed values that generated different sequences of "pseudo-random" numbers for the Monte-Carlo simulation.

Visualization of MCell simulation

To validate and verify the output of the MCell simulation, it was necessary to generate 3D renderings of the meshes (ISM and sample boxes) and particles (ions). MCell generated visualization files for use in the open-source 3D

render software, DReAMM (version 3.3). All simulation images in this manuscript were generated with DReAMM.

Mean open times were measured from single-channel gradients by hand using the cursors in Clampfit (Molecular Devices, Sunnyvale, CA). These values were used to calculate NPo, the product of the number of channels (N) and the open probability (Po), at different voltages by summing time of the events and dividing by the time range used to collect the events. NPo was calculated from transmembrane currents according to Eq. 8 of Gray (17). Best-fit alignment of single-channel gradients was performed as described earlier (18) with incorporation of the ion-trap correction factor determined in this work.

RESULTS

Response times of K^+-selective microelectrodes were determined by measuring a controlled transient change in $[K^+]$. Current injection (20 pA) through one K^+-selective microelectrode (source) was used to generate a step rise in $[K^+]$ that was measured with a second K^+-selective microelectrode, illustrated in Fig. 1 A. This method enables rapid generation of a K^+ gradient of similar magnitude to those

generated by the ion channels in this study. The noise and drift associated with flow systems prevented their use for such small changes in $[K^+]$. Fig. 2 A shows the voltage recorded by the second K^+-selective microelectrode at increasing distance from the source electrode. The profiles contain the electrical transient of the applied current step summed with the measured $[K^+]$-dependent voltage change. The magnitude of the electrical transient was independent of the distance between the source and measuring electrode and was therefore subtracted to reveal only the $[K^+]$-dependent voltage measurements in Fig. 2 B. The measuring electrode came from a batch of electrodes with inner tip diameters of 2.5–2.8 μm and was filled with a 30-μm column of K^+-selective mixture made with 2-nitrophenyl octyl ether. $[K^+]$ profiles are evident within a few micrometers from the source electrode but are barely detected at 11.5 μm from the source. The slopes of the rise times and amplitudes of the $[K^+]$-dependent voltage decrease with increasing distance from the source electrode, consistent with diffusion of K^+ away from the source electrode. We calculate a 95%
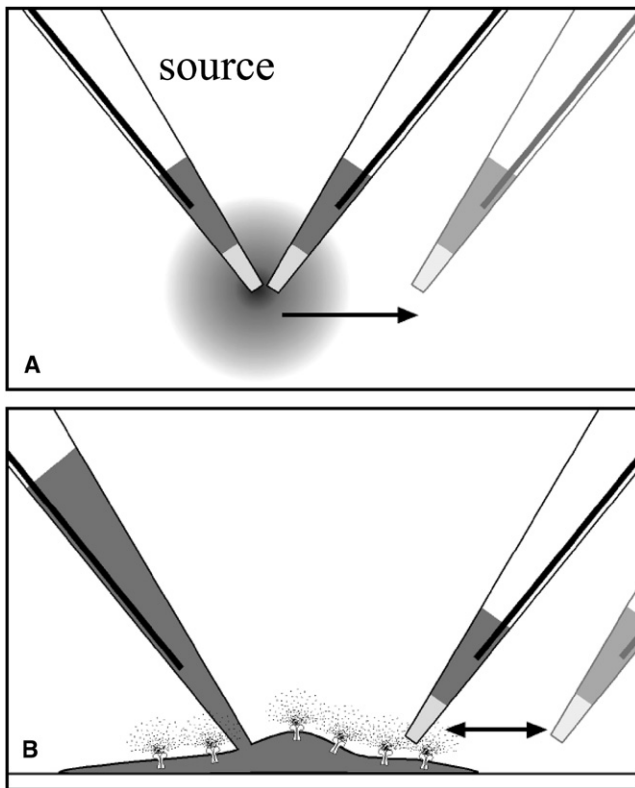

FIGURE 1 Diagrams showing the use of K^+-selective microelectrodes. (A) Current clamp of a K^+-selective microelectrode was used to generate a point source for an ion gradient of similar magnitude to those expected from single Ca^{2+}-activated K^+ channels. $[K^+]$ profiles were collected by the measuring K^+-selective microelectrode at increasing distance from the source. (B) Whole-cell voltage clamp was used to control the cytosolic $[Ca^{2+}]$ while depolarizing the membrane to activate the rSlo channels in a controlled manner. The K^+-selective microelectrode was moved in a stop-and-hold mode, coming to rest for ≤ 10 s in a position near the cell and also in a position 20 μm away from the cell.
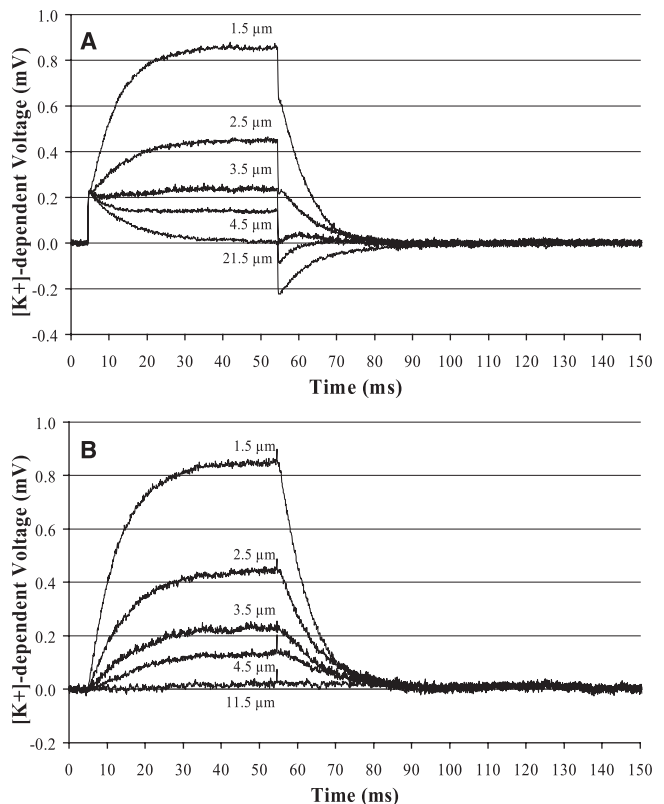

FIGURE 2 $[K^+]$ profiles measured at increasing distance from a current-clamped source K^+-selective electrode. (A) Raw voltage measurement from a K^+-selective microelectrode that contains the $[K^+]$-dependent voltage summed with a transient charge across the return electrode. The transient charge across the return electrode was independent of position in the bath and was subtracted to generate the $[K^+]$-dependent voltages alone, as shown in B. (B) The amplitude and rising and falling slopes of the $[K^+]$ profiles decrease with increasing distance from the source electrode.

response time ($t_{95\%}$) of 27 $\pm$ 1 ms for this ISM based on the measured [K^+] profiles.

Detection of single-channel ion gradients

Extracellular changes in [K^+] were monitored next to CHO cells overexpressing rSlo channels as diagrammed in Fig. 1 B. Gating of this type of channel is dependent on membrane voltage, pH_i, and [Ca^{2+}]$_i$ (19–22). Under the conditions we used, channels require a transmembrane potential of at least +40 mV to open with 200 nM [Ca^{2+}]$_i$ but will open at 0 mV in the presence of 400 nM [Ca^{2+}]$_i$. Once successful whole-cell voltage clamp was achieved, the K^+-selective microelectrode was positioned next to the edge of the cell as close as possible without touching the liquid membrane of the ISM to the plasma membrane of the cell. Measurements were obtained from cells still stuck relatively flat to the dish and on cells that had rounded up slightly. With this setup, depolarization of the plasma membrane created measurable extracellular K^+ gradients in 9 of 14 cells. Failed measurements were caused either by noisy ISMs in which the liquid membrane was not stable within the micropipette or by the ISM becoming physically blocked by debris in the culture dish. Positioning of the ISM near the membrane without touching was also a problem. Tapping the patched cell with the liquid membrane caused an instant efflux of K^+, and tapping the patched cell with the side of the ISM broke the high-resistance seal of the patch electrode.

When 200 nM [Ca^{2+}]$_i$ was used, a basal increase in K^+ was measured along with very few single-channel gradients even at +60 mV. Fig. 3 shows a recording from a cell clamped with 200 nM [Ca^{2+}]$_i$, first depolarized to +60 mV and then polarized to −60 mV, showing the difference in extracellular [K^+] between a membrane with active and then inactive channels. The basal rise in [K^+] is in part caused by the efflux of K^+
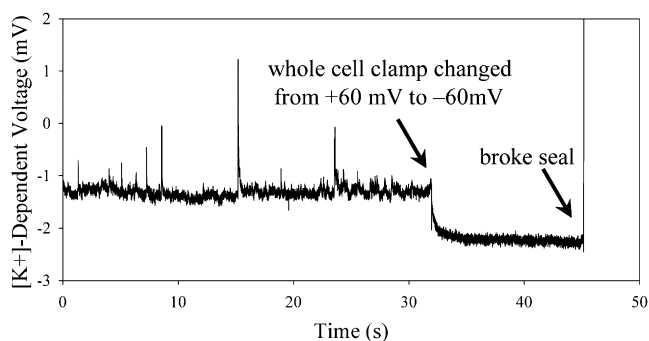

FIGURE 3 Measurement of extracellular [K^+] near the surface of a CHO cell overexpressing rSlo channels at both depolarizing and resting potentials. Depolarization was used to activate rSlo channels, giving rise to a slightly higher background [K^+] superimposed with single-channel gradients, which appear as spikes. Voltage clamping the membrane back to −60 mV led to inactivation of rSlo channels, a reduction in background [K^+], and removal of single-channel [K^+] gradients. Breaking the GΩ seal allowed K^+ to flood out of the patch electrode, leading to an immediate rise in [K^+]-dependent voltage measured by the ISM.

through activated channels but may also be caused by K^+ efflux through transporters. Superimposed on the steady increase in [K^+]-dependent voltage are large-amplitude spikes resulting from higher localized efflux of K^+ through the rSlo channels, which are not seen at the −60 mV holding potential when channels are not open. The single-channel gradients were used to calculate a mean open time of 16.9 $\pm$ 10.3 ms ($n = 65$ events) for the cell shown in Fig. 3.

With 400 nM [Ca^{2+}]$_i$, the ISM measured large basal increases in [K^+] next to the cell, >8.5 mV at +60 mV, from the high overexpression and combined activation of many of these channels. Single-channel gradients were not easily resolved under these conditions. Iberiotoxin was added to a final concentration of 300 nM to knock out a large fraction of these channels to capture single-channel gradients over a range of holding potentials. Fig. 4, A–C, show representative [K^+]-dependent voltage changes measured with an ISM near the same CHO cell, clamped to 0, +20, and +60 mV, respectively. The cell remained clamped at each potential for the duration of each recording. The ISM was moved in a stop-and-hold mode with a period of 20 s, alternating between a position near the cell and then 20 μm further away. This gave rise to the step function in the recording, measuring a greater [K^+]-dependent voltage near the cell. Similar to Fig. 3, large-amplitude spikes are superimposed on the steady increase in [K^+]-dependent voltage only when the ISM is near the cell. The frequency and mean amplitude of the spikes increase with increasing applied voltage as expected from the nature of these channels. The single-channel ion gradients are sufficiently small in the away position that they are buried within the noise. Fig. 4, D–F, show expansion of the regions under the gray bars in Fig. 4, A–C, respectively. The recording in the near position is at the same region of the cell. With low channel activity, gradients from single channels can be discretized (Fig. 4, D and E). However, with higher activity, K^+ gradients from different channel events sum together, giving rise to much larger [K^+]-dependent voltages as shown in Fig. 4 F. The inset to Fig. 4 F shows expansion of a broad spike under the gray bar in Fig. 4 F, indicating peaks from three K^+ gradients or channel events. We use the term channel events because currently we cannot resolve whether the three ion gradients originated from the same channel firing rapidly in succession or from multiple channels. The use of multiple ISMs in close proximity could give better positional information and help resolve this issue.

The single-channel gradients possess the information to enable calculation of mean open times and open probabilities. The mean open times for the events from the cell shown in Fig. 4 are 33.5 $\pm$ 7.9, 42.3 $\pm$ 18.4, and 32.6 $\pm$ 12.7 ms when the membrane potential was held at 0, 20, and 60 mV, respectively. NPo values can be determined from the ion gradient measurements as well but only reveal the value for a small patch of plasma membrane, whereas NPo values from transmembrane currents represent channels over the entire membrane. A direct comparison of these values
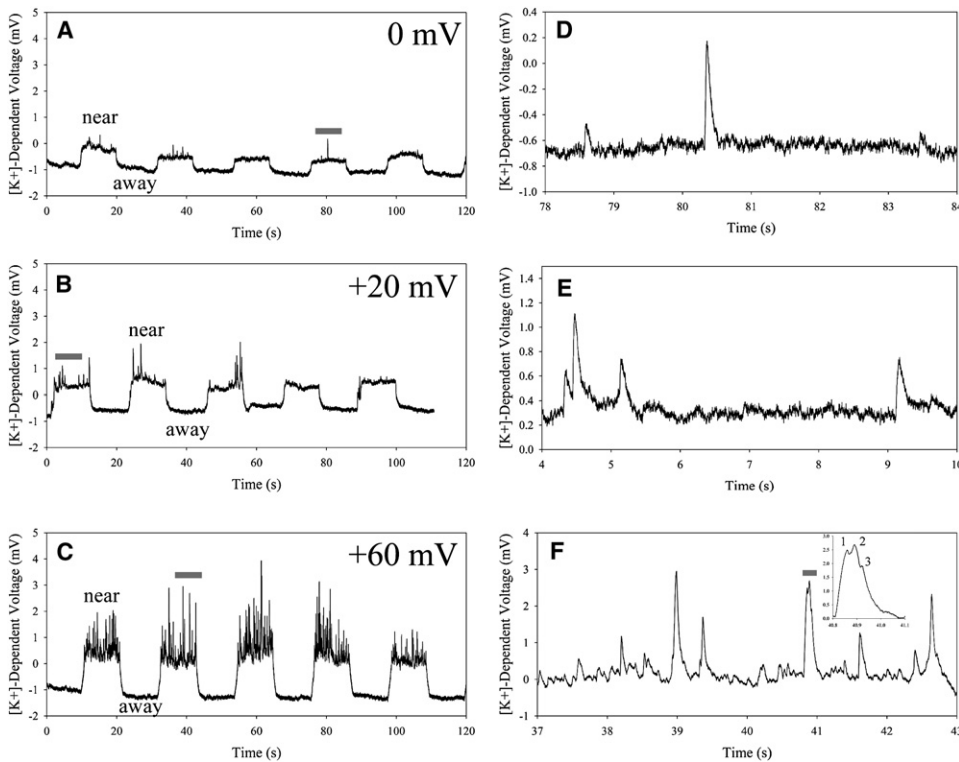
FIGURE 4 Extracellular $[K^+]$ measurements near activated rSlo channels overexpressed in a CHO cell. A fast-response K^+-selective microelectrode was repeatedly positioned at a position near the cell for 10 s and then at a position 20 μm away from the cell for 10 s. The cell was voltage clamped at 0, +20, and +60 mV (A, B, and C, respectively) to activate more channels. K^+ gradients from single channels (spikes) are captured only when the electrode is in the near position. (D–F) Expansion of regions in A, B, and C, respectively, that have been highlighted with an overlying gray bar. Single-channel gradients are easily detected at lower depolarizing potentials when fewer channels are active (D and E). Single-channel gradients sum together producing larger $[K^+]$-dependent voltages when greater channel densities are activated (F). The inset to F shows expansion of a large-amplitude event that is the sum of at least three single-channel events.

requires normalizing the ISM measured region to the entire surface area of the membrane. The calculated NP_o values from transmembrane currents are 0.1, 1.3, and 4.3 for 0, 20, and 60 mV, respectively. The corrected NP_o values determined from the ion gradient measurements are similar, 0.2, 1.3, and 4.2 at 0, 20, and 60 mV, respectively, assuming a 3-μm-diameter measuring region for the ISM and a cell diameter of 10 μm, revealing the voltage-activated nature of these channels.

Modeling of ion trapping by ISMs

Best-fit alignment of single-channel gradients was performed using a simple diffusion model and taking into account electrochemical driving force, channel open time, distance of the K^+-selective microelectrode from the channel, and response time of the measuring system, as presented earlier (18). However, these parameters were not sufficient to account for the $[K^+]$ profiles that we measured with fast response microelectrodes. Specifically, the simple diffusion model was undershooting the magnitude of the measured profiles by ~2-fold. By taking into account that the microelectrode is acting as a significant barrier to diffusion along with its close proximity to the plasma membrane, we investigated the possibility that the microelectrode is acting as an ion trap. Fig. 5 displays an illustration of the physical model and representative changes to $[K^+]$ profiles when an ideal, standard-sized ISM is positioned such that the center of the active surface is 1.5 μm away from the ion channel point source. The $[K^+]$ has been determined within a small spherical region of interest shown in Fig. 5, B–E, to closely

compare the extent of ion trapping for an ISM at three different angles, when the sensing surface of the ISM is parallel, at a 45° angle, and perpendicular to the plane of the plasma membrane, Fig. 5, C–E, respectively. Modeling of the small spherical region was used to remove the changes in $[K^+]$ that would occur because of the three different orientations of the ISM during measuring in an ion gradient. Ion trapping leads to modifications in the measured profile, as displayed in Fig. 5 F, including steeper rises and falls and higher peak concentration. The ion trap is greatest when the active surface of the ISM is both parallel and at a 45° angle to the plasma membrane. The ion trap enhances the magnitude to a lesser extent when the ISM surface is perpendicular to the plasma membrane when compared to diffusion in the absence of the ISM.

To determine the more practical influence of ion trapping on measurements, we determined the change in concentration for a thin disk (100 nm) near the active surface of the ISM. The concentration profiles for the thin disk were calculated in the presence and absence of the ISM, and the ratio of the two was calculated to assess the influence of ion trapping. Fig. 6 A shows the concentration profiles when the plane of the sensing disk is parallel to the surface of the membrane for two separation distances, 0.3 and 1.0 μm. The ratio of the profiles (presence of ISM/absence of ISM) nearly follows a step function except for a small, brief (<2 ms) overshoot that occurs at the beginning of the event (data not shown). The magnitude of this step function is plotted in Fig. 6 B for the three different configurations of the ISM surface with respect to the plasma membrane surface. The ratios are plotted against
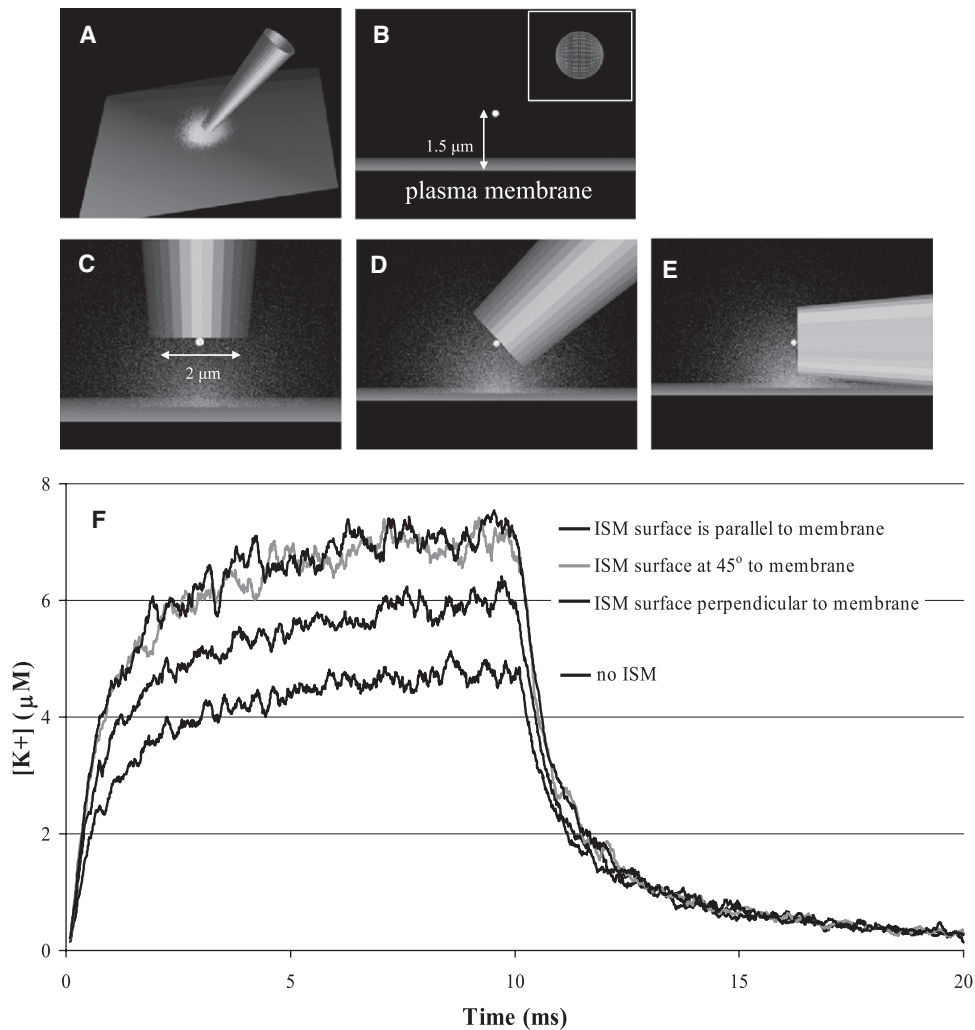
FIGURE 5 Diagram of the working ion-trap model and resultant [K$^+$] profiles for different configurations of the K$^+$-selective microelectrode. (*A*) Expanded view of the rendered microelectrode near the cell surface during the middle of K$^+$ efflux through an open channel. (*B*) Side view of the small sampling region (*white sphere,* expanded in *inset*) used to determine the [K$^+$] profile in the absence of the microelectrode. (*C–E*) Side views of the sampling region when the microelectrode active surface is parallel, at a 45° angle, and perpendicular to the plasma membrane surface. (*F*) The calculated [K$^+$]-profiles for the different configurations of the microelectrode indicate the highest amount of ion trapping when the active surface of the microelectrode is parallel and at a 45° angle to the cell surface.

the separation distance between the plasma membrane surface and the center of the active surface of the ISM. The ion trap is greatest when the active surface of the ISM is parallel and at a 45° angle to the plasma membrane surface.

These ratio values were incorporated into the simple diffusion model used by Messerli et al. (18) to perform the best-fit alignments of single-channel K$^+$ gradients from two different cells. The alignments were performed by taking into account the driving force and background extracellular [K$^+$] while varying distance of the channel from the ISM, open time, and time constant of the measuring system. Fig. 7 shows representative alignments of two channel gradients acquired under very different circumstances. The channel gradients in Fig. 7, *A* and *B*, were acquired from cells clamped at 0 mV with 400 nM [Ca^{2+}]$_i$ and clamped at +60 mV with 200 nM [Ca^{2+}]$_i$, respectively. Best-fit alignment of the ion gradient in Fig. 7 *A* indicates that the time constant of the ISM was relatively slow (65 ms) and that the channel was 0.72 μm from the center of the ISM and was open for 30 ms. Best-fit alignment of a measurement made with a concentric ISM shows a faster time constant

(29 ms) and reports that the channel was 1.03 μm from the center of the ISM and was open for 15 ms.

DISCUSSION

To map ion channels with brief open times it is critical to use ISMs with short response times. Long response times are primarily caused by the RC filtering that occurs from the ISM and the electronics (23,24). Large inner tip diameters and shorter columns of ion-selective mixture produce lower-resistance electrodes (23,25), thus reducing response times. We have employed these considerations by making microelectrodes with 2- to 3-μm inner diameters and with column lengths of 30 μm for Ca^{2+} and H$^+$ electrodes and 100 μm for K$^+$ electrodes (8). Although lowered resistance has shortened response times, parasitic capacitances remain. By increasing the thickness of the glass pipette and using a more mechanically stable K$^+$-selective mixture, we were able to produce ISMs with response times <30 ms with a 30-μm column. Shortening the column further produces electrodes with even faster response times but leads to less
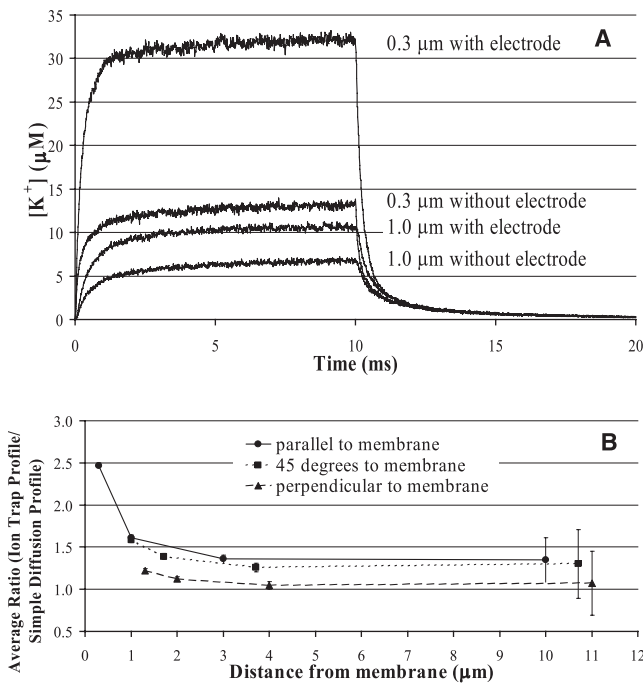
FIGURE 6 Determination of the extent of ion trapping for different microelectrode configurations with distance from the plasma membrane. (A) Theoretical [K$^+$] profiles in the presence and absence of the microelectrode when the microelectrode surface is parallel to the plasma membrane at 0.3 and 1 μm away from the plasma membrane. (B) Summary plot of the theoretical correction factors for different configurations of microelectrode at increasing distance from the plasma membrane.

FIGURE 7 Best-fit alignment of theoretical [K$^+$]-dependent voltage profiles with single-channel gradient voltage measurements. The best-fit alignment is overlaid on the recording to enable direct comparison. The model incorporated both simple diffusion and the distance-dependent correction factor caused by ion trapping.

stable electrodes. A unique, more complicated design to reduce column length also has the side effect of reducing capacitance. Instead of simply placing a backfilling solution behind the ion-selective mixture, a second inner pipette, filled with electrolyte, is run up near the tip. This design produced K$^+$-selective ISMs with time constants of 1.5–7 ms for three different ion-selective mixtures (11). This method has recently been used to produce ISMs with response times <10–20 ms for Ca^{2+} and H$^+$ electrodes, respectively, in the absence of any significant interfering ions (12). Mathematical methods such as deconvolution can also be employed to correct the recording for the relatively slow response times of the ISMs (26).

Functional mapping of ion channels with ISMs requires that the channels be active and that the electrochemical driving force for the permeant ions is not at equilibrium. Larger extracellular K$^+$ gradients will be generated when the electrochemical potential is further away from the K$^+$ equilibrium potential. Here we used voltage clamp to depolarize the plasma membrane while controlling cytosolic [Ca^{2+}] to activate the rSlo channels at less positive depolarizing potentials. By controlling the electrochemical driving force and knowing the channel conductance, we were able to measure single-channel gradients in a controlled manner. The information contained within the mapped ion gradients enabled relative localization of active rSlo channels and equivalent determina-
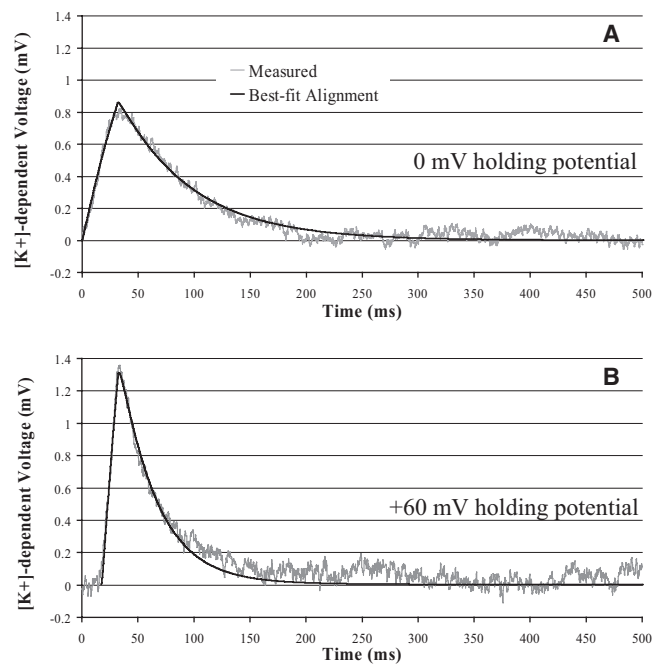
tion of NPo compared to the NPo determined from the transmembrane currents. However, the slow response time of the ISM prevented detection of events shorter than ~10 ms, leading to overestimation of mean open time by three- to five-fold when compared to earlier reports (22). This selection for longer events was also evident in Fig. 4 as the mean open time did not increase with increasing applied voltage.

The ISM was moved in a step-and-hold mode, translating between a position close to the cell and one further away. This method, known as self-referencing, enables characterization of the noise of the system so that it can be removed from the noisy signal. In conjunction with spectral filtering, self-referencing can be used to increase the signal/noise ratio by subtracting the average power spectrum of the noise from the signal of interest. Spatial self-referencing would be useful for measurements on cells and tissues ex vivo, where there is extra space to move the ISM and characterize the system noise. Temporal self-referencing would be more useful on electrically excitable cells where there are intermittent signals, allowing for the collection of noise between signals.

The ion gradients measured here with fast-response ISMs did not fit a simple diffusion model as reported earlier for slow-response ISMs (18). The primary difference is that the rapid response ISMs record a more accurate [K$^+$] profile, leaving less room for flexibility in the modeling parameters. The ion trap introduces amplification of the small, brief events that other ion-mapping techniques do not possess. Not only should this enhance characterization of channels

that generate extracellular gradients through efflux, but it should have a similar effect of enhancing characterization of channels that generate inverted gradients from ionic influx, such as Na^+ and Ca^{2+} channels. Although ion trapping makes it easier to detect single-channel gradients, it poses a potential artifact for measurements where simple diffusion is assumed to predominate. Specifically, ion trapping could lead to an overestimate of ion flux that is calculated when performing self-referencing of ISMs. By using the electrode in a configuration where the active surface of the ISM is perpendicular to the membrane surface, this overestimate can be minimized.

In future works it may be important to determine the exact position of the channel with respect to the position of the ISM(s). This will provide sufficient information to enable the identification of the channel conductance and conductance changes without previous knowledge of channel characteristics. Currently the best placement of an ion channel that we can perform with a single electrode will put the channel somewhere along the surface of a hemisphere with the ISM at the center of its radius of curvature. If the plane of the plasma membrane is known, the hemisphere reduces to the circle or oval where the hemisphere and plane intersect. This can be achieved with a double-barreled microelectrode where one barrel serves as the ISM and the other (an open barrel) is used to map distance to the membrane with impedance feedback. A more complicated multibarrel design employs two ISMs to measure the gradient and a third open barrel for impedance feedback. Information collected from this triple-barreled configuration would enable placement of the channel along the line of intersection of the two ISM measuring hemispheres, a semicircle, intersected by the plasma membrane plane generated by the impedance feedback microelectrode. This reduces the location of the channel to two possible points. Careful modeling must be used to determine the level of distortion that a multibarreled electrode would impose to the diffusion gradient. This mode of detection could prove very useful when mapping channels of similar ionic permeabilities but different conductances.

The method outlined here will work best on electrically excitable cells and tissues where relatively large signals would occur for even brief channel open times as the membrane potential changes over a wide range. Channel mapping and characterization could occur through the many forms of extracellular or intracellular electrical stimulation as well as chemical and mechanical activation. Continuous mixing on the outside of the cells must be avoided, as it will disrupt the ion gradient. The method is also suited for use on cells with extracellular layers that do not significantly interfere with diffusion of the ions. We were able to functionally map mSlo channels on *Xenopus* oocytes that were still enclosed in the coelomic envelope (18).

REFERENCES

1. Hille, B. 2001. Ion Channels of Excitable Membranes. Sinauer Associates, Sunderland, MA.

2. Roberts, W. M., and W. Almers. 1992. Patch voltage clamping with low-resistance seals: loose patch clamp. *Methods Enzymol.* 207: 155–176.

3. Korchev, Y. E., Y. A. Negulyaev, C. R. W. Edwards, I. Vodyanoy, and M. J. Lab. 2000. Functional localization of single active ion channels on the surface of a living cell. *Nat. Cell Biol.* 2:616–619.

4. Demuro, A., and I. Parker. 2003. Optical single-channel recording: imaging Ca^{2+} flux through individual N-type voltage-gated channels expressed in *Xenopus* oocytes. *Cell Calcium.* 34:499–509.

5. Demuro, A., and I. Parker. 2005. Optical patch-clamping: Single-channel recording by imaging Ca^{2+} flux through individual muscle acetylcholine receptor channels. *J. Gen. Physiol.* 126:179–192.

6. Haugland, R. P. 2005. The Handbook: A Guide to Fluorescent Probes and Labelling Technologies. Invitrogen, Carlsbad, CA.

7. Messerli, M. A., K. R. Robinson, and P. J. S. Smith. 2006. Electrochemical sensor applications to the study of molecular physiology and analyte flux in plants. *In* Plant Electrophysiology. A. G. Volkov, editor. Springer, Berlin, Heidelberg, New York, pp. 73–107.

8. Smith, P. J. S., R. H. Sanger, and M. A. Messerli. 2007. Principles, development and applications of self-referencing electrochemical microelectrodes to the determination of fluxes at cell membranes. *In* Electrochemical Methods for Neuroscience. A. C. Michael and L. M. Borland, editors. CRC Press, Boca Raton, FL, pp. 373–405.

9. Smith, P. J. S., K. Hammar, D. M. Porterfield, R. H. Sanger, and J. R. Trimarchi. 1999. Self-referencing, non-invasive, ion selective electrode for single cell detection of trans-plasma membrane calcium flux. *Microsc. Res. Tech.* 46:398–417.

10. Ammann, D., C. Pingsan, and W. Simon. 1987. Valinomycin-based K^+ selective microelectrodes with low electrical membrane resistance. *Neurosci. Lett.* 74:221–226.

11. Ujec, E., O. Keller, N. Křiž, V. Pavlík, and J. Machek. 1980. Low-impedance, coaxial, ion-selective, double-barrel microelectrodes and their use in biological measurements. *J. Electroanal. Chem.* 116: 363–369.

12. Fedirko, N., N. Svichar, and M. Chesler. 2006. Fabrication and use of high-speed, concentric H^+- and Ca^{2+}-selective microelectrodes suitable for *in vitro* extracellular recording. *J. Neurophysiol.* 96:919–924.

13. Messerli, M. A., P. J. S. Smith, R. C. Lewis, and K. R. Robinson. 2004. Chloride fluxes in lily pollen tubes: a critical reevaluation. *Plant J.* 40:799–812.

14. Bers, D. M., C. W. Patton, and R. Nuccitelli. 1994. A practical guide to the preparation of Ca^{2+} buffers. *In* Methods in Cell Biology: A Practical Guide to the Study of Calcium in Living Cells. R. Nuccitelli, editor. Academic Press, San Diego, pp. 3–29.

15. Stiles, J. R., D. Van Helden, T. M. Bartol, E. E. Salpeter, and M. M. Salpeter. 1996. Miniature endplate current rise times <100 μs from improved dual recordings can be modeled with passive acetylcholine diffusion from a synaptic vesicle. *Proc. Natl. Acad. Sci. USA.* 93:5747–5752.

16. Stiles, J. R., and T. M. Bartol. 2001. Monte Carlo methods for simulating realistic synaptic microphysiology using MCell. *In* Computation Neuroscience: Realistic Modeling for Experimentalists. E. De Schutter, editor. CRC Press, London, pp. 87–127.

17. Gray, P. T. A. 1987. Analysis of whole cell currents to estimate the kinetics and amplitude of underlying unitary events: relaxation and

''noise'' analysis. *In* Microelectrode Techniques. D. Ogden, editor. The Company of Biologists, Cambridge.

18. Messerli, M. A., E. D. Corson, and P. J. S. Smith. 2007. Measuring extracellular ion gradients from single channels with ion-selective microelectrodes. *Biophys. J.* 92:L52–L54.

19. Laurido, C., S. Candia, D. Wolff, and R. Latorre. 1991. Proton modulation of a Ca^{2+}-activated K^+ channel from rat skeletal muscle incorporated into planar bilayers. *J. Gen. Physiol.* 98:1025–1043.

20. Butler, A., S. Tsunoda, D. P. McCobb, A. Wei, and L. Salkoff. 1993. mSlo, a complex mouse gene encoding ''maxi'' calcium-activated potassium channels. *Science.* 261:221–224.

21. Ha, T. S., S. Y. Jeong, S. -W. Cho, H. -k. Jeon, G. S. Roh, et al. 2000. Funtional characteristics of two BK_{Ca} channel variants differentially expressed in rat brain tissues. *Eur. J. Biochem.* 267:910–918.

22. Barrett, J. N., K. L. Magleby, and B. S. Pallotta. 1982. Properties of single calcium-activated potassium channels in cultured rat muscle. *J. Physiol.* 331:211–230.

23. Ammann, D. 1986. Ion-Selective Microelectrodes. Springer-Verlag, Berlin.

24. Bakker, E., P. Bühlmann, and E. Pretsch. 1997. Carrier-based ion-selective electrodes and bulk optodes. 1. General characteristics. *Chem. Rev.* 97:3083–3132.

25. Orme, F. W. 1969. Liquid ion-exchanger microelectrodes. *In* Glass Microelectrodes. M. Lavalleé, O. F. Schanne, and N. C. Hébert, editors. John Wiley & Sons, New York, pp. 376–395.

26. Tucker, J. L., R. Wen, and B. Oakley, II.. 1991. A deconvolution technique for improved estimation of rapid changes in ion concentration recorded with ion-selective microelectrodes. *IEEE Trans. Biomed. Eng.* 38:156–160.